RSC Advances

ROYAL SOCIETY OF CHEMISTRY

www.rsc.org/advances

N-doped graphene quantum dots as effective photocatalyst for the photochemical synthesis of silver doposited porous graphitic C_3N_4 nanocomposites for nonenzymatic electrochemical H_2O_2 sensing

Deli Jiang*, Yuan Zhang, Haoyu Chu, Jie Liu, Jin Wan, and Min Chen*

School of Chemistry and Chemical Engineering, Jiangsu University, Zhenjiang 212013, P. R. China

Corresponding author:

Tel.: +86 51188791708; Fax: +86 511 88791800

E-mail: dlj@ujs.edu.cn, chenmin3226@sina.com

Abstract:

In this work, nitrogen-doped graphene quantum dots (N-GQDs) were proved to be an efficient photocatalyst for photochemical synthesis of Ag nanoparticles loaded porous graphitic C_3N_4 (p-g-C_3N_4) for the first time. The Ag nanoparticles were well-formed in high yield and closely anchored at the surface of p-g-C_3N_4 with uniform size distribution. Importantly, as-prepared Ag/p-g-C_3N_4 nanocomposites exhibited excellent catalytic activity towards electrocatalytic reduction of hydrogen peroxide (H_2O_2). The cyclic voltammetry and amperometry results show that the sensor of as-prepared Ag/p-g-C_3N_4 composite exhibit excellent analytical response to H_2O_2 with fast response, wide linear range and low detection limit.

1 Introduction

Graphitic carbon nitride, referred to as g-C_3N_4, possesses a stacked two-dimensional structure and is the most stable allotrope of carbon nitride under ambient conditions.[1] In addition, g-C_3N_4 is abundant and easily-synthesized via one-step polymerization of the cheap feedstocks like cyanamide, dicyandiamide, melamine, thiourea and urea.[2-5] Its graphene-like sp^2 bonding structure, together with abundant in-plane nitrogen dopants and defects, gives it an appealing electronic structure, which is responsible for its multifunctional catalytic activity for a broad variety of reactions, including water splitting, CO_2 reduction, organic degradation, etc.[6-8] In our previous reports, heterojunction photocatalysts (BiOI/porous g-C_3N_4, Ag_3PO_4/porous g-C_3N_4) with execllent visible-light-driven photocatalytic peformance have been sucessfully fabricated.[9,10]

On the other hand, N-containing carbons have received considerable attentions due to the strong electron donor nature of N which should promote enhancement in π bonding, leading to improved stability, electron transfer rate, and enhance durability of the carbon supports during electrocatalytic processes.[11] Because of its rich pyridine-like nitrogens content and facile synthesis procedure, g-C_3N_4 may provide more active reaction sites than other N-carbon materials towards electrocatalytic applications.[12] Recently, g-C_3N_4 as electrocatalyst in fuel cells and other electrochemical applications has been gradually studied extensively.[13-16] Barman and co-workers fabricated two-dimensional C_3N_4 sheets through a bottom-up method for electrochemical sensing of mercuric ions.[17] Sun *et al.* reported that ultrathin g-C_3N_4 nanosheets directly prepared by ultrasonication-assisted liquid exfoliation of bulk

g-C_3N_4 can be used as a low-cost and efficient electrocatalyst toward the reduction of H_2O_2.[18] However, these synthetic approaches suffer from relatively low yield and poor reproducibility. Furthermore, despite these efforts, g-C_3N_4 alone still shows limited electrocatalytic activity.

Fluorescent carbon nanodots (CDs) and graphene quantum dots (GQDs) have attracted much attention due to their unique properties and wide applications in photocatalyst, bio-imaging, ion detection, and electrochemical luminescence.[19-22] It has been found recently that CDs or GQDs could also be used as a green reductant or support to synthesize CDs-metal nanocomposites.[23-25] We have sucessfully synthesized Ag/C/Ag core-shell-satallite nanocomposites by using nitrogen-doped CDs prepared from biomass as reductant, which exhibited excellent surface-enhanced Ramman scattering properties.[26] Kim and co-workers synthesized carbon dots-supported silver nanoparticles (NPs) (CDs-Ag NPs) using the carbon dots both as a reducing agent and a template under ultraviolet irradiation to fabricate solution-processable polymer light-emitting diodes and polymer solar cells.[27] The excellent electron-donating capability of photoexcited CDs enables fast reduction of metal salts to corresponding metal nanoparticles on the surfaces of the CDs. Sun et. al demonstrated that CDs can be served as an effective photocatalyst for fabricating AuNPs-rGO nanocomposites by UV irradiation of a mixture of GO and $HAuCl_4$ aqueous solution in the presence of CDs.[28]

Herein, we report a facile and green synthsis of silver NPs deposited porous g-C_3N_4 (Ag/p-g-C_3N_4) using nitrogen-doped GQDs (N-GQDs) as effective photocatalyst. The

Ag/p-g-C_3N_4 nanocomposites were obtained simply by visible light irridation of the mixture of g-C_3N_4 and $AgNO_3$ aqueous solution in the presence of N-GQDs. To the best of our knowledge, the use of N-GQDs as a photocatalyst for photocatalytic deposition has never been reported before. Importantly, the resultant Ag/p-g-C_3N_4 nanocomposites exhibited excellent catalytic activities towards electrocatalytic hydrogen peroxide (H_2O_2) reduction. In addition, the as-fabricated Ag/p-g-C_3N_4 modified glassy carbon electrode (GCE) as a nonenzymatic H_2O_2 sensor showed high sensitivity and low detection limit.

2 Experimental

2.1 Materials

Citric acid, urea, hydrogen peroxide (H_2O_2, 30 wt%) and ethanol were purchased from Sinopharm Chem. Reagent Co., Ltd (Shanghai, China). Silver nitrate ($AgNO_3$) were purchased from Aldrich Chemical Comp. All chemicals were used as received without further purification. The water used was double-distilled after a deionized exchange.

2.2 Preparation of p-g-C_3N_4

p-g-C_3N_4 were prepared according to the method we reported previously,[9] and the details are described as follows. p-g-C_3N_4 was synthesized by thermal treatment of 10 g of urea in a crucible with a cover under ambient pressure in air. After drying at 80 °C for 24 h, the precursor was heated to 550 °C at a heating rate of 2.3 °C min^{-1} in a tube furnace for 4 h in air. The resulting final light yellow powder was washed with nitric acid (0.1 mol L^{-1}) and distilled water to remove any residual alkaline species (e.g. ammonia) adsorbed on the sample surface, and then dried at 80 °C for 24 h.

2.3 Preparation of N-GQDs

N-GQDs were synthesized according to the method reported previously.[29] Typically, 0.525 g (2.5 mmol) citric acid and 0.45 g (7.5 mmol) urea were dissolved into 12 ml water, and stirred to form a clear solution. Then the solution was transferred into 50 ml Teflon lined stainless autoclave. The sealed autoclave was heated to 160 ℃ in an electric oven and kept for additional 8 hours. The final product was collected by adding ethanol into the solution and centrifuged at 5000 rpm for 5 min. The solid can be easily redispersed into water.

2.4 Preparation of Ag/p-g-C_3N_4

In a typical preparation, 0.1 g of p-g-C_3N_4 powders were added into 10 mL of 0.5 mg mL^{-1} as-prepared N-GQDs dispersion. After 30 min stirring at room temperature, the suspension were added into a quartz tube, followed by addition of 50 mL of 11.8 mM $AgNO_3$ solution. Prior to irradiation, the suspension was magnetically stirred in the dark for another 30 min. The mixture was irradiated under visible light obtained by using cut off filters to remove light (150 W, Xenon lamp) of $\lambda < 420$ nm for 1 h under magnetic stirring (note: cooling water was circulated outside the reactor to maintain the reaction temperature at 25 ℃). After irradiation, the brown precipitates were collected by centrifugation at the speed of 8000 rpm and washed with deionized water and ethanol for 3 times, respectively, finally dried under vacuum at 60 ℃ for 12 h before further characterization. For comparasion, the Ag deposited p-g-C_3N_4 in the absence of N- GQDs (denoted as a-Ag/p-g-C_3N_4) was also synthesized using the same method except for prolonging the irradiation time to 6 h.

2.5 Preparation of the modified electrode and electrochemical measurements

1.0 mg of Ag/p-g-C_3N_4 composite and 10 µl of Nafion solution (5 wt%) were dispersed in 1 mL water-isopropanol mixed solvent (3:1 v/v) by at least 30 min sonication to form a homogeneous catalyst solution. Then 10 µL of the catalyst solution was dropped onto the surface of pretreated GCE and left to dry at room temperature to get Ag/p-g-C_3N_4-modified GCE, referred to as Ag/p-g-C_3N_4/GCE. Amperometric and cyclic voltammetry (CV) experiments were carried out by a CHI 650D electrochemical analyzer (CH Instruments, Inc., Shanghai), in a home-made three-electrode electrochemical cell consisting of a twisted platinum wire as an auxiliary electrode, a saturated calomel electrode (SCE) as a reference electrode and a modified-GCE (0.07 cm^2) as a working electrode. All experiments were carried out at the ambient temperature. Prior to the experiment, The electrolyte, consisting of a solution of 0.2 M phosphate buffer solution (PBS, pH 7.4), was purged with high-purity nitrogen for at least 30 min and a nitrogen atmosphere was maintained over the solution.

2.6 Characterization

Purity and crystallization of the samples were characterized by powder X-ray diffraction on a D/max–γA X-ray spectrometer (Rigaku, Japan) at 40 kV and 200 mA with monochromatic Cu Kα (λ=1.5418 Å) radiation. Transmission electron microscopy (TEM) images were taken on a TECNAI12 TEM instrument (Philips) with an accelerating voltage of 200 kV. Scanning electron micrograph (SEM) and energy dispersive X-ray analysis (EDX) spectroscopy were taken on a field emission SEM (FESEM) instrument (Hitachi S-4800 II, Japan). The surface areas of the sample

was measured by a TriStar II 3020-BET/BJH Surface Area. X-ray photoelectron spectroscopy (XPS) was performed on a VG-ADES 400 instrument with Mg K-ADES source. Elemental analyses (C, N and O) were performed with a Vario MICRO CHNOS Elemental Analyzer. Metal elemental analyses were carried out by inductively coupled plasma spectroscopy (ICP, Optima2000DV, USA) analysis. Electrochemical measurements were performed with a CHI 650D electrochemical analyzer (CH Instruments, Inc., Shanghai).

3 Results and discussion

3.1 Morphology and structure of the Ag/p-g-C_3N_4 composite

XRD was used to identify and determine the phase structures of the as-prepared samples. As shown in Fig. 1a, the XRD pattern of the p-g-C_3N_4 sample reveals two distinct diffraction peaks at 27.50° and 13.04° corresponding to the (002) and (100) diffraction planes of the graphite-like carbon nitride, which is consistent with the standard value (JCPDS 87−1526).[30] Fig. 1b shows the XRD pattern of the Ag deposited p-g-C_3N_4 synthesized using the same method in the absence of N-GQDs (denoted as: a-Ag/p-g-C_3N_4). It can be found that the diffraction intensity of the peaks at 27.50° and 13.04° become weaker, additionally, related to the metallic Ag are hardly found, which may be due to the low doping levels of Ag NPs in a-Ag/p-g-C_3N_4. In spite of shorter irradiation time, compared with a-Ag/p-g-C_3N_4, as-prepared Ag/p-g-C_3N_4 (curve c) exhibit four additional peaks located at 38.0, 44.2, 64.3, and 77.3° corresponding to 111, 200, 220, and 311 faces of Ag, respectively. These observations suggest that N-GQDs serve as an effective photocatalyst for the

formation of Ag photo-deposited p-g-C_3N_4.

Fig. 2 shows FE-SEM images of the pure p-g-C_3N_4, a-Ag/p-g-C_3N_4 and Ag/ p-g-C_3N_4 nanocomposites. The morphology of the pure p-g-C_3N_4 is consisted of thin sheet-like with wrinkles and irregular shape (Fig. 2a), which is the typical structure characteristic of g-C_3N_4 synthesized by the polymerization of urea.[31] After photo-deposition of silver NPs on the p-g-C_3N_4, it can be seen that the morphology of p-g-C_3N_4 remained intact and a few small sphere-like nanoparticles were dispersed on its surface (Fig. 2b). Fig. 2c,d show the FE-SEM images of the Ag/p-g-C_3N_4 synthesized in the presence of N-GQDs. It is observed that a large amount of Ag NPs with diameters in the range 10-20 nm are uniformly and densely generated on the p-g-C_3N_4. In addition, the EDX spectrum of Ag/p-g-C_3N_4 reveals the presence of elements of C, N and Ag (Note that: the presence of element Si was generated from the supporting Si substrate for decreasing the charging effects under the SEM-imaging conditions). These results provide another piece of evidence to support the formation of Ag nanoparticles after irradiation.

In order to study the microstructure of the Ag/p-g-C_3N_4 in more detail, transmission electron microscopy (TEM) and high-resolution transmission electron microscopy (HRTEM) observations were carried out. As presented in Fig. 3a, the morphology of the pure p-g-C_3N_4 is composed of a large lamellar structure, and a number of mesopores of several tens of nanometres in size can be observed in the p-g-C_3N_4 sheets, which was highly analogous to previously reported results.[32] In comparasion with TEM image of a-Ag/p-g-C_3N_4 (Fig. 3b), more Ag NPs with a narrow size

distribution were observated on the surface of p-g-C_3N_4 in Fig. 3c. At high magnification TEM image (Fig. 3d), it can be found that the Ag nanoparticles are approximately spherical in shape and anchored on the p-g-C_3N_4. The HRTEM image taken from the nanoparticle (insert in Fig. 3d) reveals clear lattic fringes with an interplane distance of 0.238 nm corresponding to the (111) lattice space of metallic Ag, further revealing the nanoparticle is Ag. These results are consistent with above XRD and EDX observations.

To learn more about the porous nature and specific surface area of the as-prepared Ag/p-g-C_3N_4 composite, a nitrogen adsorption-desorption isotherm was measured. Fig. 4 shows the isotherm for the sample, which exhibits a type IV with a H3 hysteresis loop according to the IUPAC classification, reflecting the presence of a mesoporous structure of the composites. It can be found that the synthesized Ag/p-g-C_3N_4 composite shows a relatively large specific surface area (21.98 $m^2\ g^{-1}$), which is close to the BET surface area of the pure p-g-C_3N_4 synthesized according to our previous reports (23.19 $m^2\ g^{-1}$).[9,10] The pore-size distribution of the sample is also estimated using the Barrett-Joyner-Halenda (BJH) method from the desorption branch of the isotherm, as shown in the inset of Fig. 4. The calculated pore size distribution using BJH method indicates that the size of mesopores is not uniform ranging from 8 to 50 nm, which is consistent with the TEM observation. And the average pore size of the Ag/p-g-C_3N_4 composite is estimated to be 14.59 nm, which is also close to the average pore size of the p-g-C_3N_4 (13.64 nm).[9,10]

X-ray photoelectron spectroscopy (XPS) surface probe technique can further

confirm the surface composition and elements of the resultant Ag/p-g-C_3N_4 composite. Fig. 5 shows the survey XPS of the hybrid, which is mainly dominated by the signals of C, N, O, and Ag. The accurate percentage ratio of C : N : O : Ag further determined by elemental analyzer and ICP analysis was estimated to be 40.12 : 50.09 : 5.71 : 4.08. Fig. 6a presents the Ag XPS spectrum of the sample. The strong peaks at 368.3 and 374.4 eV can be ascribed to the binding energies of the Ag $3d_{5/2}$ and $3d_{3/2}$ electrons ofmetallic Ag(0). Fig. 6b shows the XPS of Ag/p-g-C_3N_4 in the N 1s binding energy regions, and the spectrum can be fitted into three peaks at 398.9, 399.7 and 401.1 eV, which are attributed to pyridinic, pyrrolic and quaternary N, respectively.[33-35] The C1s spectrum (Fig. 6c) has been deconvoluted into four peaks at 284.9, 287.6, 288.5, 289.0 eV, assigned to sp^2 C atoms bonded to N in an aromatic ring (N−C=N), sp^3 hybridized C atoms (C-$(N)_3$), C-O (hydroxyl and epoxy carbon) and C=O (carboxylic carbon) , respectively.[36,37] And the O1s spectrum (Fig. 6d) decomposed at 531.2, 532.8 eV are assigned to O-C and O=C, which can be ascribed to the oxygenous groups of the residual N-GQDs on the surface of Ag/p-g-C_3N_4. These results also indicate the strong interaction between the N-GQDs and p-g-C_3N_4.

Based on all of above experimental results, the photochemical synthesis of Ag/p-g-C_3N_4 nanocomposites can be possibly explained as follows. Firstly, the N-GQDs can be adsorbed effectively onto p-g-C_3N_4 due to their similar CN heterocyclic structures and the strong interaction between carboxyl groups of N-GQDs and amino groups of p-g-C_3N_4.[26,29,38,39] These oxygenous groups and amino groups also played an important role in adsorbing and stabilizing Ag^+ ions,[27,39,40] thus

Ag^+ ions can be anchored uniformly on the surface of p-g-C_3N_4. During the photochemical synthetic process, N-GQDs acted as a photosensitizer because of their broad visible light absorption under visible light.[29] N-GQDs can absorb the visible light, and then the electron is excited to excited state.[28,29,41-43] Subsequently, the photogenerated electrons from N-GQDs inject to the p-g-C_3N_4 and simultaneously reduce the surrounding Ag^+ to Ag^0, finally resulting in the formation of Ag NPs deposited p-g-C_3N_4 composite.[28,29] Actually, this successful and efficient preparation can be ascribed to the excellent electron-donating capability of photoexcited N-GQDs.[27] In the photochemical synthetic process, the N-GQDs essentially not only act as a catalyst but also perform as a reducing agent. The schematic illustration of the proposed mechanism for the photochemical synthesis of the Ag/p-g-C_3N_4 nanocomposite is shown in Scheme 1.

3.2 Electrochemical sensing of H_2O_2

Hydrogen peroxide (H_2O_2), a well-known oxidizing agent, is not only a by-product of a large number of oxidase enzymes, but also an essential mediator in food, pharmaceutical, clinical, industrial and environmental analysis.[44] Electrochemical H_2O_2 sensors, especially nonenzymatic amperometric biosensors, have attracted extensive attention due to their high sensitivity, simplicity, good compatibility and long term stability.[45-47] The promising application as an enzyme-free biosensor for H_2O_2 was selected as a preliminary test of the electrocatalytic behaviors of as-prepared Ag/p-g-C_3N_4 nanocomposites.

To testify the sensing application of Ag/p-g-C_3N_4 nanocomposites, an enzymeless

H_2O_2 sensor was constructed by direct deposition of the aqueous dispersion of Ag/p-g-C_3N_4 nanocomposites on a bare GCE surface. The cyclic voltammograms of the bare GCE, p-g-C_3N_4/GCE, a-Ag/p-g-C_3N_4/GCE and Ag/p-g-C_3N_4/GCE in N_2 saturated 0.2 M pH 7.4 PBS containing 5.0 mM H_2O_2 are shown in Fig. 7. It can be obviously seen that the responses of both the bare GCE and p-g-C_3N_4/GCE towards the reduction of H_2O_2 are quite weak. The a-Ag/p-g-C_3N_4/GCE shows a good response towards the reduction of H_2O_2 due to the presence of Ag nanoparticles, but no obvious current peak is observed. In contrast, the Ag/p-g-C_3N_4/GCE exhibits a remarkable catalytic current peak about 238 μA in intensity at -0.52 V vs. SCE. The above results indicate that as-prepared Ag/p-g-C_3N_4 has a good electrocatalytic activity towards the H_2O_2 reduction and the high number density Ag NPs with narrow size distribution anchored on the p-g-C_3N_4 play an important role as the main electroactive materials.

It should be noted that the Ag/p-g-C_3N_4/GCE exhibits a 260 mV and 100 mV positive shift of the peak potential compared to Ag NPs-modified GCE by electrodeposition technique[48] and hydrothermal synthesis of PQ11-Ag NPs decorated GCE,[49] respectively. In addition, the as-prepared Ag/p-g-C_3N_4 modified GCE shows good repeatability with a relative standard deviation (RSD) of 3.8 % for five successive detections at 5.0 mM H_2O_2. Also, the current response retained 92 % of its initial value after a storage period of 3 weeks, indicating the good long-term stability of the Ag/p-g-C_3N_4 composites.

Under optimal conditions, a typical current-time plot of a Ag/p-g-C_3N_4 composite

modified electrode upon successive additions of aliquots of H_2O_2 is shown in Fig. 8a. To avoid or decrease the interference of other electro-active species and minimize the background current, an applied potential of -0.3 V was used for the amperometric determination of H_2O_2.[50] As H_2O_2 is added to the stirred PBS solution, well-defined steady state current responses are obtained within 2 s at the applied potential, and the current increases stepwise with successive additions of H_2O_2.

The current response displays a good liner behavior in a concentration range from 0.1 to 39.5 mM with a correlation coefficient of 0.999 (as shown in Fig. 8b). And the the detection limit is estimated to be 0.6 μM at a signal-to-noise ratio of 3. Notably, our present sensing system shows a lower detection limit than most of those sensors for detection of H_2O_2, such as AgNPs (1.0 μM),[51] PEDOT/AgNPs (7.0 μM),[52] AgNPs/DNA (1.7 μM),[53] AgNPs/PQ11/GN (28 μM),[54] AgNPs/rGO (31.3 μM),[55] AgNPs-CDs (0.5 μM),[25] nitrogen-doped carbon nanotubes (0.37 μM).[56] Taking advantage of its cheaper and easier preparation approach, as-prepared Ag/p-g-C_3N_4 composite is an excellent choice for construction of enhanced electrochemical sensing platform.

From these results, the well-dispersed Ag NPs and the p-g-C_3N_4 support show a synergistic effect on the superior electrocatalytic activity. The mechanism for H_2O_2 electro-reduction can be expressed as follows:[56]

$$H_2O_2 + e^- \rightarrow OH_{ad} + OH^- \quad (1)$$

$$OH_{ad} + e^- \rightarrow OH^- \quad (2)$$

$$2OH^- + 2H^+ \rightarrow 2H_2O \quad (3)$$

The formation of OH_{ad} (i.e. chemisorbed OH) is a key step controlling the reaction rate in the reduction of H_2O_2.[57] For as-prepared Ag/p-g-C_3N_4 composite modified electrode, the well-dispersed Ag NPs with high number density and their surfactant-free surface attributed to the green synthestic approach could make the main contributions to the observed excellent catalytic activity.[38] The pyridinic nitrogen in the p-g-C_3N_4 support also play an important role in enhancing its electrocatalytic activity.[58,59] In addition, the excellent electrochemical sensing performance of as-synthesized Ag/p-g-C_3N_4 composite could be also attributed to its relatively large specific surface area and porosity.

For practical applications, we also investigate the selectivity of the Ag/p-g-C_3N_4 composite modified electrode for H_2O_2 detection. Ascorbic acid (AA), uric acid (UA) and glucose (Glu) are three common electroactive substances and commonly present in physiological samples, so interfering effect of AA, UA and Glu on the amperometric response of Ag/p-g-C_3N_4/GCE toward H_2O_2 was investigated. As shown in Fig. 9. a well-defined current response is observed for H_2O_2 while no obvious current responses to 1.0 mM AA, 1.0 mM UA and 2.0 mM Glu are observed, which is largely attributed to the relatively low applied potential of -0.3 V used in the determination of H_2O_2.[50] The observation indicates that the electrode could be applied to the selective determination of H_2O_2 in real samples.

4 Conclusions

In summary, N-doped GQDs has been proved to be an efficient photocatalyst for photochemical synthesis of Ag NPs loaded p-g-C_3N_4 for the first time. The FESEM and TEM images of Ag/p-g-C_3N_4 composite revealed that Ag NPs were well-formed in high yield and closely anchored at the surface of p-g-C_3N_4 with uniform size

distribution. Moreover, the cyclic voltammetry and amperometry results show that the electrochemical sensor of as-prepared Ag/p-g-C_3N_4 composite exhibit excellent analytical response to H_2O_2 with fast response, wide linear range and low detection limit. Importantly, this method opens up a green photocatalytic synthesis of noble metal NPs/p-g-C_3N_4 nanocomposites for sensing and other applications.

Acknowledgments

This work was supported by the financial supports of Jiangsu Planned Projects for Postdoctoral Research Funds (1202040C), College Natural Science Research Program of Jiangsu Province (13KJB610003), Zhenjiang Industry Supporting Plan (GY2013023), Zhenjiang Social Developing Plan (SH2013002), Research Foundation for Talented Scholars of Jiangsu University (11JDG149 and 10JDG133) and Jiangsu Innovation Training Program Plan for College Students (201310299055Y).

Reference

1 M. Groenewolt and M. Antonietti, *Adv. Mater.*, 2005, **17**, 1789.

2 X. C. Wang, K. Maeda, A. Thomas, K. Takanabe, G. Xin, J. M. Carlsson, K. Domen and M. Antonietti, *Nat. Mater.*, 2009, **8**, 76.

3 Y. W. Zhang, J. H. Liu, G. Wu and W. Chen, *Nanoscale*, 2012, **4**, 5300.

4 J. S. Zhang, M. W. Zhang, R. Q. Sun and X. C. Wang, *Angew. Chem. Int. Ed.*, 2012, **51**, 10145.

5 Y. J. Wang, Z. X. Wang, S. Muhammad and J. He, *CrystEngComm*, 2012, **14**, 5065.

6 F. Dong, L. W. Wu, Y. J. Sun, M. Fu, Z. B. Wu and S. C. Lee, *J. Mate. Chem.*, 2011, **21**, 15171.

7 Y. Cui, J. Huang, X. Fu and X. Wang, *Catal. Sci. Technol.*, 2012, **2**, 1396.

8 Y. Q. Shi, S. H. Jiang, K. Q. Zhou, B. B. Wang, B. Wang, Z. Gui, Y. Hu and R. K. Yuen, *RSC Adv.*, 2014, **4**, 2609.

9 D. L. Jiang, L. L. Chen, J. J. Zhu, M. Chen, W. D. Shi and J. M. Xie, *Dalton Trans.*,

2013, **42**, 15726.

10 D. L. Jiang, J. J. Zhu, M. Chen and J. M. Xie, *J. Colloid Interface Sci.*, 2014, **417**, 115.

11 Y. F. Zhang, X. J. Bo, A. Nsabimana, C. Luhana, G. Wang, H. Wang, M. Li and L. P. Guo, *Biosens. Bioelectron.*, 2014, **53**, 250.

12 Y. Zheng, Y. Jiao, J. Chen, J. Liu, J. Liang, A. Du, W. Zhang, Z. Zhu, S. C. Smith, M. Jaroniec, G. Q. Lu and S. Z. Qiao, *J. Am. Chem. Soc.*, 2011, **133**, 20116.

13 M. Tahir, C. Cao, F. K. Butt, F. Idrees, N. Mahmood, Z. Ali, I. Aslam, M. Tanveer, M. Rizwan and T. Mahmood, *J. Mater. Chem. A*, 2013, **1**, 13949.

14 J. Liang, Y. Zheng, J. Chen, J. Liu, D. Hulicova-Jurcakova, M. Jaroniec and S. Z. Qiao, *Angew. Chem., Int. Ed.*, 2012, **51**, 3892.

15 K. Kwon, Y. J. Sa, J. Y. Cheon and S. H. Joo, *Langmuir*, 2011, **28**, 991.

16 J. Jin, X. Fu, Q. Liu and J. Zhang, *J. Mater. Chem. A*, 2013, **1**, 10538.

17 M. Sadhukhan and S. Barman, *J. Mater. Chem. A*, 2013, **1**, 2752.

18 J. Tian, Q. Liu, C. Ge, Z. Xing, A. M. Asiri, A. O. Al-Youbi and X. Sun, *Nanoscale*, 2013, **5**, 8921.

19 S. N. Baker and G. A. Baker, *Angew. Chem. Int. Ed.*, 2010, **49**, 6726.

20 H. Li, Z. Kang, Y. Liu and S.-T. Lee, *J. Mater. Chem.*, 2012, **22**, 24230.

21 A. Safavi, F. Sedaghati, H. Shahbaazi and E. Farjami, *RSC Adv.*, 2012, **2**, 7367.

22 Y. L. Zhang, L. Wang, H. C. Zhang, Y. Liu, H. Y. Wang, Z. H. Kang and S.-T. Lee, *RSC Adv.*, 2013, **3**, 3733.

23 M. M. Liu and W. Chen, *Nanoscale*, 2013, **5**, 12558.

24 X. Ran, H. Sun, F. Pu, J. Ren and X. Qu, *Chem. Commun.*, 2013, **49**, 1079.

25 S. Liu, B. Yu and T. Zhang, *RSC Adv.*, 2014, **4**, 544.

26 Y. Zhang, C. S. Xing, D. L. Jiang and M. Chen, *CrystEngComm*, 2013, **15**, 6305.

27 H. Choi, S.-J. Ko, Y. Choi, P. Joo, T. Kim, B. R. Lee, J.-W. Jung, H. J. Choi, M. Cha, J.-R. Jeong, I.-W. Hwang, M. H. Song, B.-S. Kim and J. Y. Kim, *Nat. Photo.*, 2013, **7**, 732.

28 X. Qin, W. Lu, A. M. Asiri, A. O. Al-Youbi and X. Sun, *Catal. Sci. Technol.*, 2013,

3, 1027.

29 D. Qu, M. Zheng, P. Du, Y. Zhou, L. Zhang, D. Li, H. Tan, Z. Zhao, Z. Xie and Z. Sun, *Nanoscale*, 2013, **5**, 12272.

30 L. Ge, C. Han and J. Liu, *J. Mater. Chem.*, 2012, **22**, 11843.

31 Y. W. Zhang, J. H. Liu, G. Wu and W. Chen, *Nanoscale*, 2012, **4**, 5300.

32 G. H. Dong and L. Z. Zhang, *J. Mater. Chem.*, 2012, **22**, 1160.

33 Y. Wang, Y. Shao, D. W. Matson, J. Li and Y. Lin, *ACS Nano*, 2010, **4**, 1790.

34 S. Kundu, T. C. Nagaiah, W. Xia, Y. Wang, S. V. Dommele, J. H. Bitter, M. Santa, G. Grundmeier, M. Bron, W. Schuhmann and M. Muhler, *J. Phys. Chem. C*, 2009, **113**, 14302.

35 S. U. Maraveedu, S. Devulapally, N. Karjule and S. Kurungot, *J. Mater. Chem.*, 2012, **22**, 23506.

36 L. Ge and C. Han, *Appl. Catal., B*, 2012, **117**, 268.

37 Y. Z. Lu,Y. Y. Jiang, W. T. Wei, H. B. Wu, M. M. Liu, L. Niu and W. Chen, *J. Mater. Chem.*, 2012, **22**, 2929.

38 M. M. Liu and W. Chen, *Nanoscale*, 2013, **5**, 12588.

39 Li. Tang, R. Ji, X. Cao, J. Lin, H. Jiang, X. Li, K. S. Teng, C. M. Luk, S. Zeng, J. Hao and S. P. Lau, *ACS Nano*, 2012, **6**, 5102.

40 Y. Li, Y. Zhao, H. Cheng, Y. Hu, G. Shi, L. Dai and L. Qu, *J. Am. Chem.Soc.*, 2012, **134**, 15.

41 Y. Yang, Y. Guo, F. Liu, X. Yuan, Y. Guo, S. Zhang, W. Guo and M. Huo, *Appl. Catal., B*, 2013, **142**, 828.

42 X. Ran, H. Sun, F. Pu, J. Ren and X. Qu, *Chem. Commun.*, 2013, **49**, 1079.

43 S. Zhuo, M. Shao and S.-T. Lee, *ACS Nano*, 2012, **6**, 1059.

44 H. Zhang, H. Huang, H. Ming, H. Li, L. Zhang, Y. Liu and Z. Kang, *J. Mater. Chem.*, 2012, **22**, 10501.

45 M. Sadhukhan, T. Bhowmik, M. K. Kundu and S. Barman, *RSC Adv.*, 2014, **4**, 4998.

46 X. Feng, R. Li, Y. Ma, R. Chen, N. Shi, Q. Fan and W. Huang, *Adv. Funct. Mater.*, 2011, **21**, 2989.

47 Y. Zhang, S. Liu, L. Wang, X. Qin, J. Tian, W. Lu, G. Chang and X. Sun, *RSC Adv.*, 2012, **2**, 538.

48 D. Kimmel, G. LeBlanc, M. Meschievitz and D. Cliffel, *Anal. Chem.*, 2012, **84**, 685.

49 W. Lu, F. Liao, Y. Luo, G. Chang and X. Sun, *Electrochim. Acta*, 2011, **56**, 2295.

50 C. Welch, C. Banks, A. Simm and R. Compton, *Anal. Bioanal. Chem*., 2005, **382**, 12.

51 V. K. Shukla, R. S. Yadav, P. Yadav and A. C. Pandey, *J. Hazard. Mater.*, 2012, **213**, 161.

52 A. Balamurugan and S.-M. Chen, *Electroanalysis*, 2009, **21**, 1419.

53 K. Cui, Y. Song, Y. Yao, Z. Huang and L. Wang, *Electrochem. Comm.*, 2008, **10**, 663.

54 S. Liu, J. Tian, L. Wang, H. Li, Y. Zhang and X. Sun, *Macromolecules*, 2010, **43**,10078.

55 S. Liu, J. Tian, L. Wang and X. Sun, *Carbon*, 2011, **49**, 3158.

56 X. Xu, S. Jiang, Z. Hu and S. Liu, *ACS Nano*, 2010, **4**, 4292.

57 G. Flätgen, S. Wasle, M. Lübke, C. Eickes, G. Radhakrishnan, K. Doblhofer and G. Ertl, *Electrochim. Acta*, 1999, 44, 4499.

58 C. Z. Zhu, J. F. Zhai and S. J. Dong, *Chem. Comm.*, 2012, **50**, 9367.

59 S. Yang, X. Feng, X. Wang and K.Müllen, *Angew. Chem., Int. Ed.*, 2011, **50**, 5339.

Figure captions:

Fig. 1 XRD patterns for the as-prepared samples: pure p-g-C_3N_4 (a), a-Ag/ p-g-C_3N_4 (b) and Ag/ p-g-C_3N_4.

Fig. 2 FE-SEM images of the pure p-g-C_3N_4 (a), a-Ag/p-g-C_3N_4 (b) and Ag/p-g-C_3N_4 (c,d), and EDX spectrum of Ag/p-g-C_3N_4 (e).

Fig. 3 TEM images of of the pure p-g-C_3N_4 (a), a-Ag/p-g-C_3N_4 (b) and Ag/p-g-C_3N_4 (c,d), and HRTEM image of one particle of Ag/p-g-C_3N_4 (insert).

Fig. 4 Nitrogen sorption isotherm and Barrett–Joyner–Halenda (BJH) pore size distribution plot (inset) of the Ag/p-g-C_3N_4 composite.

Fig. 5 XPS survey spectrum of the Ag/p-g-C_3N_4 composite.

Fig. 6 XPS spectra of the Ag/p-g-C_3N_4: (a) Ag 3d; (b)N 1s; (c) C 1s and (d) O 1s.

Fig. 7 Cyclic voltammograms (CVs) of bare GCE, p-g-C_3N_4/GCE, a-Ag/p-g-C_3N_4/GCE and Ag/p-g-C_3N_4/GCE in N_2-saturated 0.2 M PBS at pH 7.4 in the presence of 5.0 mM H_2O_2 (scan rate: 50 mV/s).

Fig. 8 (a) Typical steady-state response of the Ag/p-g-C_3N_4/GCE to successive injection of H_2O_2 into the stirred N_2-saturated 0.2M PBS at pH 7.4 (applied potential: -0.30V), and (b) the corresponding calibration curve.

Fig. 9 Current-time curves for the Ag/p-g-C_3N_4/GCE exposed to AA, UA (1.0 mM), glucose (2 mM) and H_2O_2 (1 mM) each.

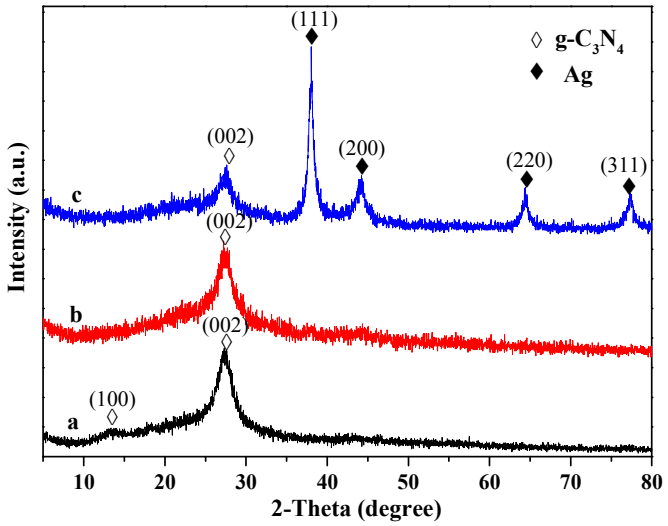

Fig. 1

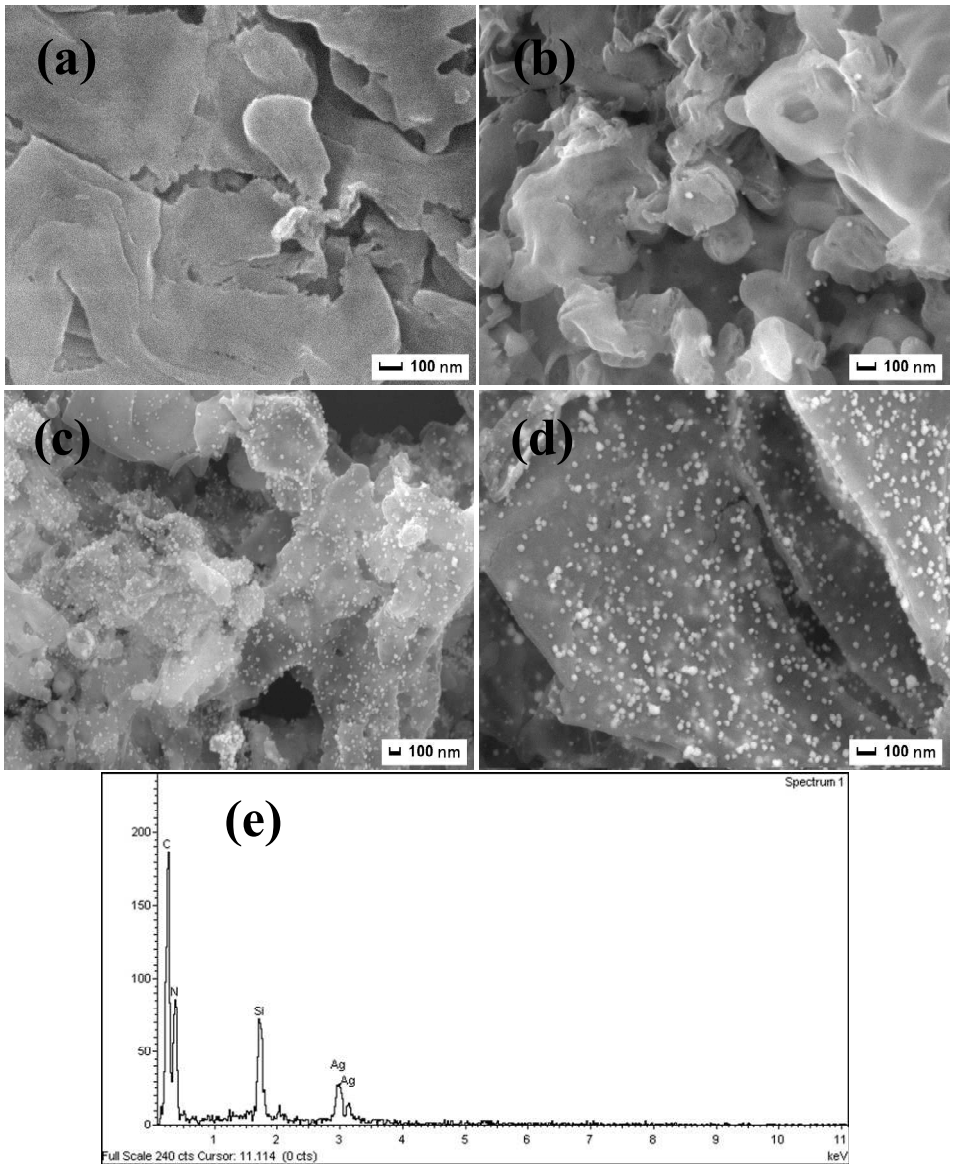

Fig. 2

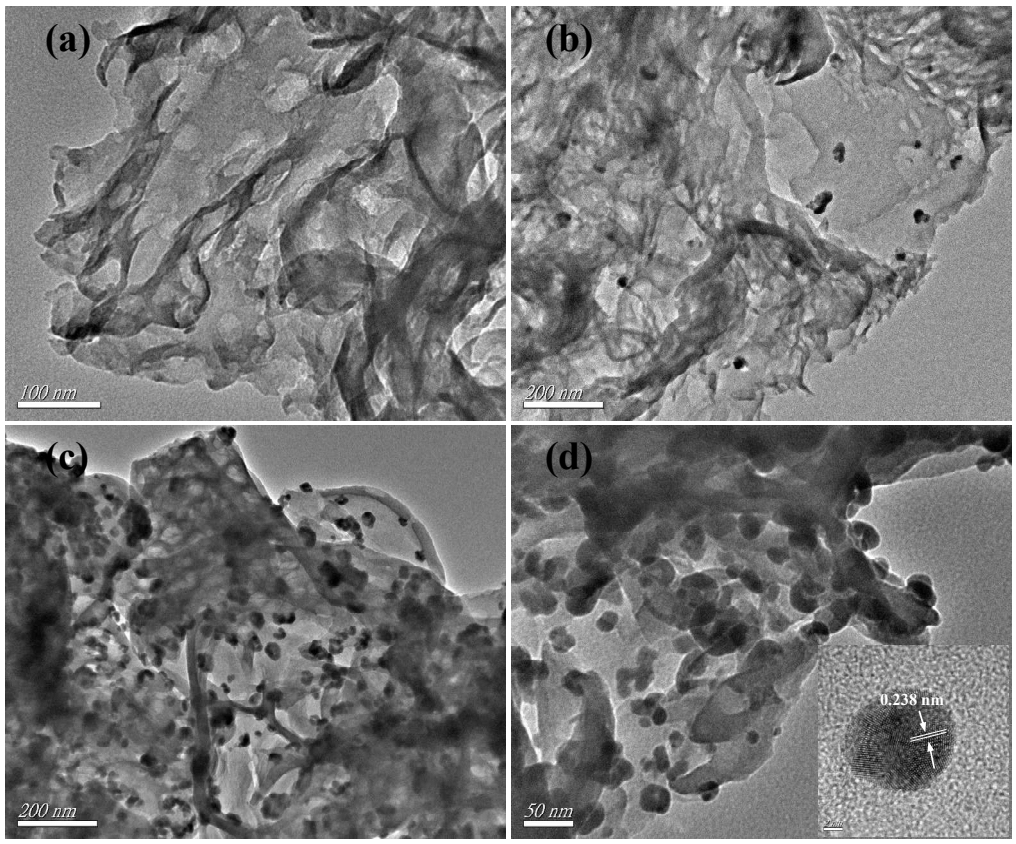

Fig. 3

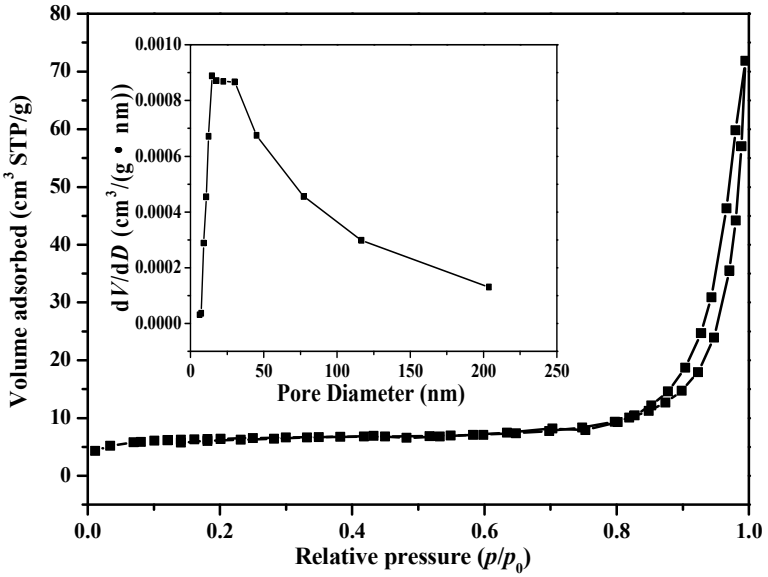

Fig. 4

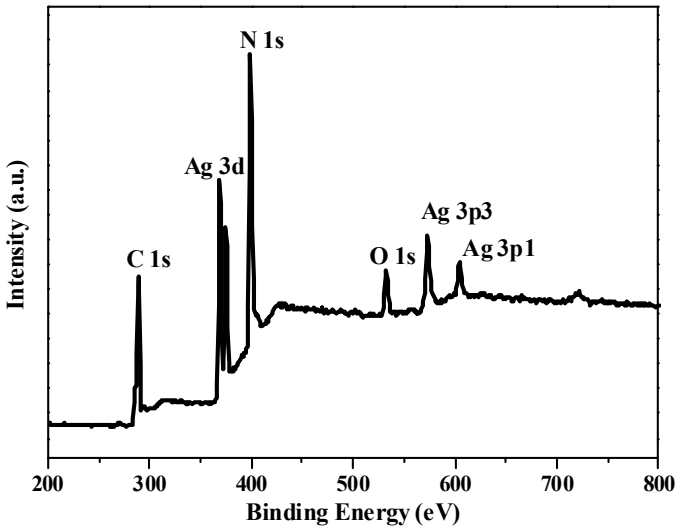

Fig. 5

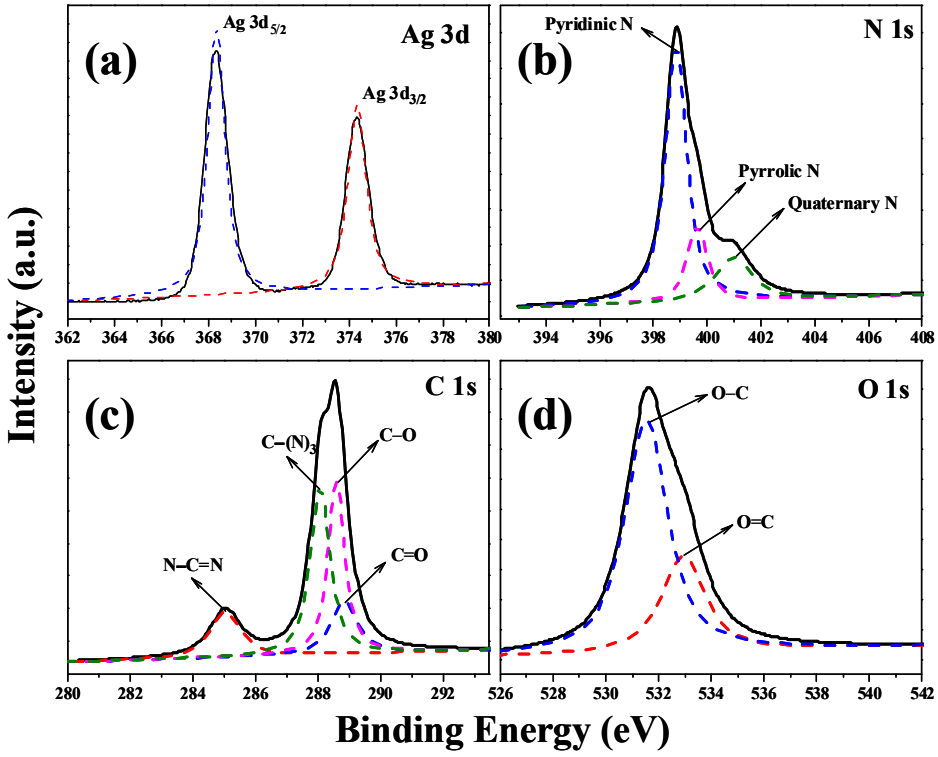

Fig. 6

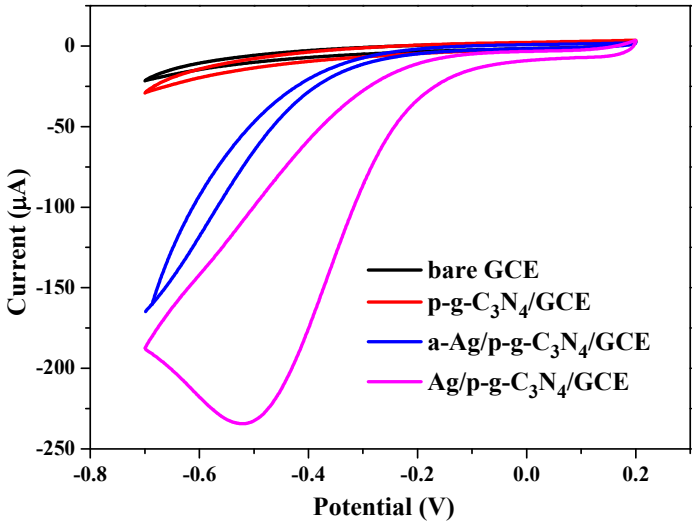

Fig. 7

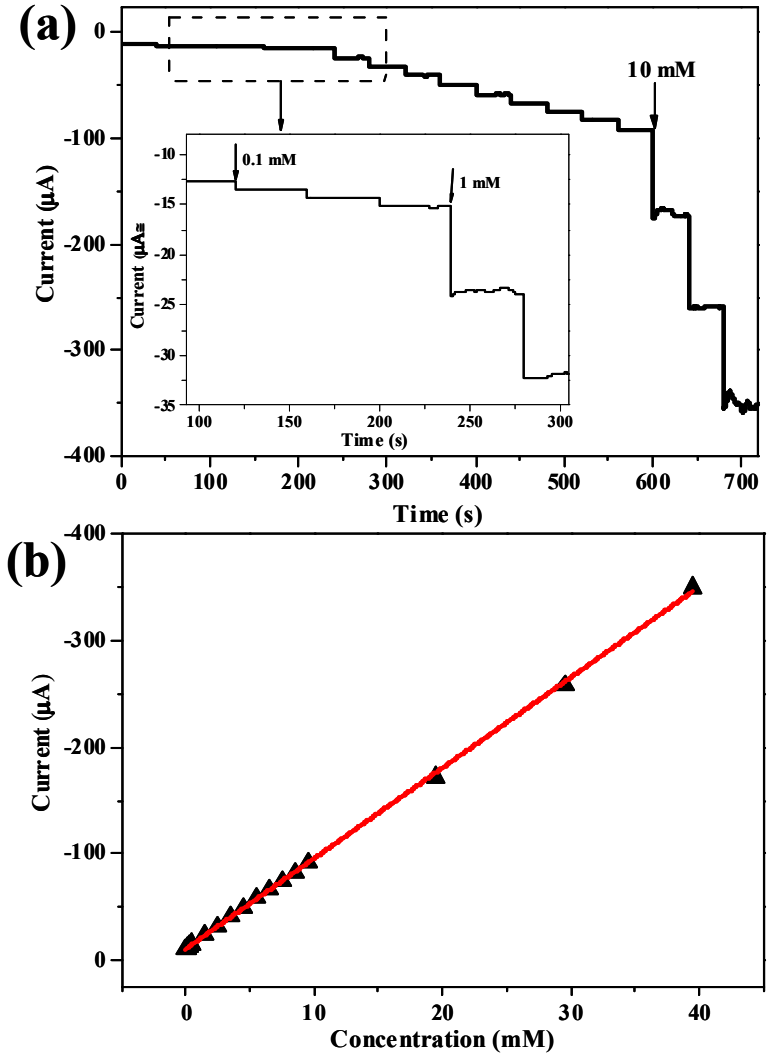

Fig. 8

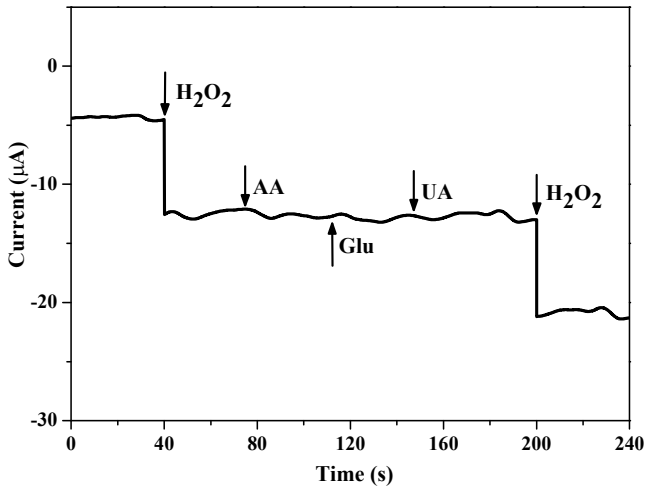

Fig. 9

Scheme captions:

Scheme 1 A schematic diagram illustrating the proposed mechanism for the photochemical synthesis of Ag/p-g-C_3N_4 nanocomposites.

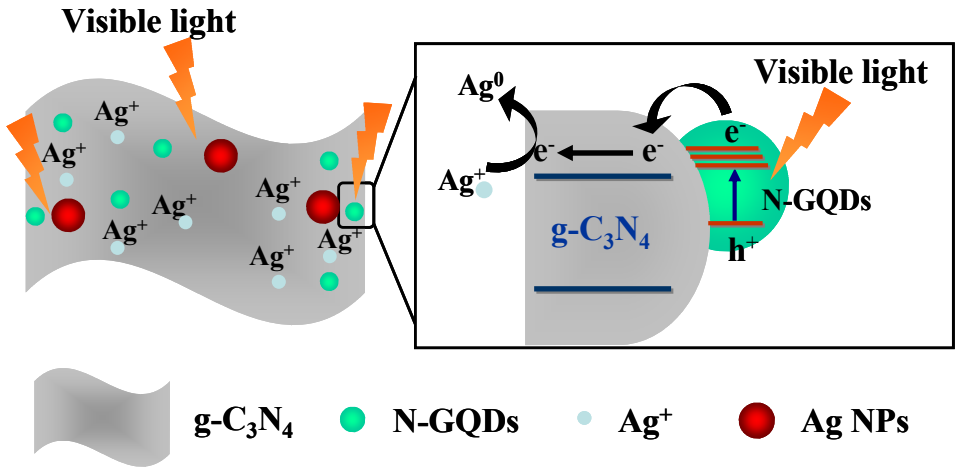

Scheme 1

N-doped GQDs served as an effective photocatalyst for the photochemical synthesis of silver doposited porous g-C_3N_4 nanocomposites for electrochemical sensing.